JOURNAL OF GUIDANCE, CONTROL, AND DYNAMICS
Vol. 18, No. 4, July–August 1995

Optimal Low-Thrust Three-Dimensional Earth–Moon Trajectories

Craig A. Kluever*
University of Missouri–Columbia/Kansas City, Kansas City, Missouri 64110-2499
and
Bion L. Pierson†
Iowa State University, Ames, Iowa 50011-3231

Minimum-fuel, three-dimensional trajectories from a circular low Earth parking orbit to an inclined circular low lunar parking orbit with a fixed thrust–coast–thrust engine sequence are computed for a low-thrust spacecraft. The problem is studied in the context of the classical restricted three-body problem. The minimum-fuel transfer to a polar lunar orbit is obtained by successively solving a sequence of fixed lunar inclination problems. Minimum-fuel three-dimensional transfers to a polar lunar orbit with meridian plane constraints are also computed. The minimum-fuel trajectory problems are solved using a "hybrid" direct/indirect method. The hybrid method utilizes the costate time histories to parameterize the three-dimensional thrust steering angle time histories. Numerical results are presented for the optimal three-dimensional Earth–moon trajectories.

Introduction

IT has been established that spacecraft propelled by low-thrust engines are capable of delivering a greater payload fraction compared to spacecraft using conventional chemical propulsion systems.[1,2] Recent low-thrust research has involved a range of piloted and cargo lunar and Mars missions.[3,4] Aston[5] has advocated the use of low-thrust propulsion for establishing a permanent lunar colony.

London[6] and Stuhlinger[7] performed early preliminary studies on low-thrust transfers from a low Earth parking orbit to a low lunar parking orbit. In each study, the low-thrust transfer consists of separate Earth and moon two-body trajectories patched together at the sphere of influence. More recently, Golan and Breakwell,[8] Enright and Conway,[9] and Pierson and Kluever[10] have investigated minimum-fuel, Earth–moon trajectories. All three studies utilized trajectories influenced by the simultaneous gravity fields of Earth and the moon. Golan and Breakwell[8] investigated both planar and three-dimensional minimum-fuel transfers for power-limited spacecraft that resulted in variable thrust–magnitude trajectories with no coasting arcs. Enright and Conway[9] demonstrated a collocation method by determining a single minimum-fuel, low-thrust, planar, Earth–moon transfer. Pierson and Kluever[10] obtained minimum-fuel, planar, Earth–moon trajectories with constant thrust magnitude and a structured thrust–coast–thrust engine sequence.

This paper extends our earlier work on optimal planar transfers[10] to a minimum-fuel problem for a three-dimensional transfer from a circular, low Earth parking orbit (LEO) in the Earth–moon plane to an inclined, circular, low lunar parking orbit (LLO). Since the Earth–moon orbital plane precesses with a period of about 18.6 years, the inclination of the moon's orbit with respect to Earth's equator varies between 18.3 and 28.6 deg. Therefore, our approach does not consider a specific launch date; instead, the initial inclination of the LEO is fixed in the Earth–moon plane and a general 90 deg plane change to a polar LLO is investigated. For current launch capabilities, a launch vehicle steering performance penalty would be incurred for launch into the assumed LEO; we do not treat this aspect of the problem. Both free and specified final meridian plane cases are considered. The three-dimensional LEO–LLO transfer is assumed to consist of a continuous-thrust, Earth-escape, spiral trajectory phase followed by a translunar coast phase and finally a continuous-thrust, moon-capture, spiral trajectory phase. All three segments are allowed to be fully three dimensional. Numerical results are presented for an electric propulsion spacecraft in the low thrust-to-weight (T/W) ratio and "moderate" equivalent power regimes.

Received June 17, 1994; revision received Oct. 13, 1994; accepted for publication Nov. 6, 1994.

*Assistant Professor, Department of Mechanical and Aerospace Engineering. Member AIAA.
†Professor, Department of Aerospace Engineering and Engineering Mechanics. Associate Fellow AIAA.

System Models

Equations of Motion

The Earth–moon trajectory is governed by the classical restricted three-body problem dynamics.[11] The three-dimensional equations of motion for the vehicle are presented in both Earth-centered and moon-centered rotating, spherical coordinate systems with the Earth–moon plane as the x–y or primary plane. The complete equations of motion for the powered Earth-escape phase are

$$\dot{r}_1 = v_{r_1} \tag{1}$$

$$\dot{v}_{r_1} = \frac{-\mu_e}{r_1^2} - \frac{\mu_m(r_1 + D\cos\phi_1\cos\theta_1)}{r_{\text{moon-S/C}}^3} + \frac{\mu_m\cos\phi_1\cos\theta_1}{D^2} + a_{T_1}\sin u_1\cos v_1 + 2\omega v_{\theta_1}\cos\phi_1 + \omega^2 r_1\cos^2\phi_1 + \frac{v_{\theta_1}^2}{r_1} + \frac{v_{\phi_1}^2}{r_1} \tag{2}$$

$$\dot{v}_{\theta_1} = \frac{\mu_m D\sin\theta_1}{r_{\text{moon-S/C}}^3} - \frac{\mu_m\sin\theta_1}{D^2} + a_{T_1}\cos u_1\cos v_1 + 2\omega v_{\phi_1}\sin\phi_1 - 2\omega v_{r_1}\cos\phi_1 - \frac{v_{r_1}v_{\theta_1}}{r_1} + \frac{v_{\theta_1}v_{\phi_1}\sin\phi_1}{r_1\cos\phi_1} \tag{3}$$

$$\dot{v}_{\phi_1} = \frac{\mu_m D\sin\phi_1\cos\theta_1}{r_{\text{moon-S/C}}^3} - \frac{\mu_m\sin\phi_1\cos\theta_1}{D^2} + a_{T_1}\sin v_1 - 2\omega v_{\theta_1}\sin\phi_1 - \omega^2 r_1\sin\phi_1\cos\phi_1 - \frac{v_{r_1}v_{\phi_1}}{r_1} + \frac{v_{\theta_1}^2\sin\phi_1}{r_1\cos\phi_1} \tag{4}$$

$$\dot{\theta}_1 = \frac{v_{\theta_1}}{r_1\cos\phi_1} \tag{5}$$

$$\dot{\phi}_1 = \frac{v_{\phi_1}}{r_1} \tag{6}$$

where

$$r_{\text{moon-S/C}} = \left(r_1^2 + 2Dr_1\cos\phi_1\cos\theta_1 + D^2\right)^{\frac{1}{2}}$$

$$a_{T_1} = \frac{T}{m_{\text{LEO}} - \dot{m}t} \qquad 0 \le t \le t_e$$

The equations of motion for the translunar coast phase are also referred to the Earth-centered coordinate frame:

$$\dot{r}_2 = v_{r_2} \tag{7}$$

$$\dot{v}_{r_2} = \frac{-\mu_e}{r_2^2} - \frac{\mu_m(r_2 + D\cos\phi_2\cos\theta_2)}{r^3_{\text{moon-S/C}}} + \frac{\mu_m\cos\phi_2\cos\theta_2}{D^2} + 2\omega v_{\theta_2}\cos\phi_2 + \omega^2 r_2\cos^2\phi_2 + \frac{v_{\theta_2}^2}{r_2} + \frac{v_{\phi_2}^2}{r_2} \tag{8}$$

$$\dot{v}_{\theta_2} = \frac{\mu_m D\sin\theta_2}{r^3_{\text{moon-S/C}}} - \frac{\mu_m\sin\theta_2}{D^2} + 2\omega v_{\phi_2}\sin\phi_2 - 2\omega v_{r_2}\cos\phi_2 - \frac{v_{r_2}v_{\theta_2}}{r_2} + \frac{v_{\theta_2}v_{\phi_2}\sin\phi_2}{r_2\cos\phi_2} \tag{9}$$

$$\dot{v}_{\phi_2} = \frac{\mu_m D\sin\phi_2\cos\theta_2}{r^3_{\text{moon-S/C}}} - \frac{\mu_m\sin\phi_2\cos\theta_2}{D^2} - 2\omega v_{\theta_2}\sin\phi_2 - \omega^2 r_2\sin\phi_2\cos\phi_2 - \frac{v_{r_2}v_{\phi_2}}{r_2} + \frac{v_{\theta_2}^2\sin\phi_2}{r_2\cos\phi_2} \tag{10}$$

$$\dot{\theta}_2 = \frac{v_{\theta_2}}{r_2\cos\phi_2} \tag{11}$$

$$\dot{\phi}_2 = \frac{v_{\phi_2}}{r_2} \tag{12}$$

Finally, the equations of motion for the powered moon-capture phase are referred to a moon-centered coordinate frame:

$$\dot{r}_3 = v_{r_3} \tag{13}$$

$$\dot{v}_{r_3} = \frac{-\mu_m}{r_3^2} - \frac{\mu_e(D\cos\phi_3\cos\theta_3 - r_3)}{r^3_{\text{Earth-S/C}}} - \frac{\mu_e\cos\phi_3\cos\theta_3}{D^2} + a_{T_3}\sin u_3\cos v_3 + 2\omega v_{\theta_3}\cos\phi_3 + \omega^2 r_3\cos^2\phi_3 + \frac{v_{\theta_3}^2}{r_3} + \frac{v_{\phi_3}^2}{r_3} \tag{14}$$

$$\dot{v}_{\theta_3} = -\frac{\mu_e D\sin\theta_3}{r^3_{\text{Earth-S/C}}} + \frac{\mu_e\sin\theta_3}{D^2} + a_{T_3}\cos u_3\cos v_3 + 2\omega v_{\phi_3}\sin\phi_3 - 2\omega v_{r_3}\cos\phi_3 - \frac{v_{r_3}v_{\theta_3}}{r_3} + \frac{v_{\theta_3}v_{\phi_3}\sin\phi_3}{r_3\cos\phi_3} \tag{15}$$

$$\dot{v}_{\phi_3} = -\frac{\mu_e D\sin\phi_3\cos\theta_3}{r^3_{\text{Earth-S/C}}} + \frac{\mu_e\sin\phi_3\cos\theta_3}{D^2} + a_{T_3}\sin v_3 - 2\omega v_{\theta_3}\sin\phi_3 - \omega^2 r_3\sin\phi_3\cos\phi_3 - \frac{v_{r_3}v_{\phi_3}}{r_3} - \frac{v_{\theta_3}^2\sin\phi_3}{r_3\cos\phi_3} \tag{16}$$

$$\dot{\theta}_3 = \frac{v_{\theta_3}}{r_3\cos\phi_3} \tag{17}$$

$$\dot{\phi}_3 = \frac{v_{\phi_3}}{r_3} \tag{18}$$

where

$$r_{\text{Earth-S/C}} = \left(r_3^2 - 2Dr_3\cos\phi_3\cos\theta_3 + D^2\right)^{\frac{1}{2}}$$

$$a_{T_3} = \frac{T}{m(t_e) - \dot{m}[t-\tau]} \qquad \tau \le t \le t_f$$

The states for all three sets of differential equations are radial position r, radial velocity v_r, longitudinal-plane velocity v_θ, latitude-plane velocity v_ϕ, longitude angle θ, and latitude angle ϕ and are denoted by the six-element vector x. The longitude θ is the angle of the projection of the radius vector onto the Earth–moon plane measured positive counterclockwise from the Earth–moon line. The latitude ϕ is measured positive above the Earth–moon orbit plane to the spacecraft radius vector. The subscripts 1, 2, and 3 indicate values with respect to the powered Earth-escape phase, coast phase, and moon-capture phase, respectively. The gravitational parameters of Earth and the moon are represented by μ_e and μ_m, respectively, ω is the constant angular rotation rate of the Earth–moon system, and D is the constant separation distance between Earth and the moon. The thrust steering angle u is measured positive above the local horizontal plane to the projection of the thrust vector onto the local longitude-radial direction vertical plane. The thrust steering angle v is measured positive above the local vertical plane to the thrust vector and is between ±90 deg. The thrust acceleration of the spacecraft, a_T, is computed by dividing the constant thrust magnitude T by the current spacecraft mass. The mass of the spacecraft is denoted by m , and propellant mass flow rate $\dot{m}$ is considered positive out of the vehicle. The durations of the powered Earth-escape and moon-capture phases are denoted by t_e and t_c, respectively, and t_f is the final time. The initiation of the moon-capture phase is at $t = \tau$, where $\tau = t_f - t_c$.

Vehicle Model

The spacecraft characteristics are from Ref. 10, where they were derived from ion propulsion lunar cargo vehicles developed by London[6] and Stuhlinger.[7] The total initial mass of the spacecraft in LEO, m_{LEO}, is fixed at 100,000 kg; the constant thrust magnitude $T = 2942$ N; and the constant mass flow rate $\dot{m} = 107.5$ kg/h. Although the assumed propulsion technology is not consistent with current capabilities, this model results in a "moderate" low-thrust vehicle with an initial T/W ratio of 3×10^{-3}. Also, we do not address the question of actually achieving the assumed initial mass in LEO with current launch capabilities. The low-thrust engines are assumed to operate without a transient tail-off or start-up period, and therefore T and $\dot{m}$ are considered to be at their respective constant values during powered flight or at zero during the coast phase.

Trajectory Optimization

Problem Statement

For the free end-time problem, find the initial longitude angle $\theta_1(0)$; the thrust steering time histories $u_1(t)$ and $v_1(t)$, $0 \le t \le t_e$, and $u_3(t)$ and $v_3(t)$, $\tau \le t \le t_f$; and the powered flight durations t_e and t_c, which minimize

$$J = t_e + t_c = \Phi[t_e, t_c, x(t_f), t_f] \tag{19}$$

subject to the three-dimensional, restricted three-body equations of motion [Eqs. (1–18)] with the boundary conditions at $t = 0$,

$$r_1(0) = r_{\text{LEO}} \tag{20}$$

$$v_{r_1}(0) = 0 \tag{21}$$

$$v_{\theta_1}(0) = \sqrt{\mu_e/r_{\text{LEO}}} - \omega r_{\text{LEO}} \tag{22}$$

$$v_{\phi_1}(0) = 0 \tag{23}$$

$$\phi_1(0) = 0 \tag{24}$$

the boundary conditions at $t = t_e$

$$x_2(t_e) = x_1(t_e) \tag{25}$$

the boundary conditions at $t = \tau$

$$x_3(\tau) = g(x_2(\tau), D) \tag{26}$$

and the terminal state constraints

$$\psi[x_3(t_f), t_f] = \begin{bmatrix} r_3(t_f) - r_{\text{LLO}} \\ v_{r_3}(t_f) \\ v_{\theta_l}^2(t_f) + v_{\phi_l}^2(t_f) - v_{cir}^2 \\ v_{\theta_l}(t_f)\cos\phi_3(t_f) - v_{cir}\cos i \end{bmatrix} = \begin{bmatrix} 0 \\ 0 \\ 0 \\ 0 \end{bmatrix} \tag{27}$$

Note that this is a "mixed" optimal control problem that involves both control functions and control parameters. The initial state conditions [Eqs. (20–24)] define the initial low Earth circular orbit with zero inclination. Therefore, the initial orbit is contained in the Earth–moon orbit plane. Equation (25) represents the required state matching conditions at the end of the Earth-escape phase ($t = t_e$) between the powered and coasting trajectory segments. Equation (26) enforces the required state matching conditions between the Earth-centered coasting arc and the moon-centered powered capture trajectory. The functional relationship $g(x_2(\tau), D)$ represents the required coordinate transformation between the two rotating frames and is detailed in Appendix A. For comparison, observe that this problem involves dynamic constraints of order 18 rather than 12 and four control functions rather than two for the earlier planar problem.[10]

The four terminal state constraints [Eq. (27)] define a circular LLO with a specified inclination i with respect to the Earth–moon plane. The terminal state constraints are expressed in the moon-centered, rotating, spherical coordinate system. The first three state constraints specify a low lunar circular orbit, and the constant v_{cir} is the circular orbital speed for the desired final radial distance r_{LLO}. The fourth state constraint ensures termination in an orbit with the desired inclination. The velocities v_{θ_I} and v_{ϕ_I} represent, respectively, inertial velocity components along the local longitude and latitude planes with respect to a fixed, moon-centered, spherical frame. Utilizing the relationship between velocities in a fixed reference frame and a rotating reference frame,

$$\boldsymbol{v}_{\text{fix}} = \boldsymbol{v}_{\text{rot}} + \boldsymbol{\omega} \times \boldsymbol{r} \tag{28}$$

we obtain the inertial velocity components

$$v_{\theta_I} = v_{\theta_3} + \omega r_3 \cos\phi_3 \tag{29}$$

$$v_{\phi_I} = v_{\phi_3} \tag{30}$$

Finally, since ω is a constant for the restricted three-body problem and the final radius $r_3(t_f)$ is constrained, the product ωr_3 is defined as a constant n. Therefore, the final two terminal state constraints in Eq. (27) are rewritten in terms of velocity components in the rotating frame:

$$\psi_3 = v_{\theta_3}^2(t_f) + n^2\cos^2\phi_3(t_f) + 2v_{\theta_3}(t_f)n\cos\phi_3(t_f) + v_{\phi_3}^2(t_f) - v_{cir}^2 = 0 \tag{31}$$

$$\psi_4 = v_{\theta_3}(t_f)\cos\phi_3(t_f) + n\cos^2\phi_3(t_f) - v_{cir}\cos i = 0 \tag{32}$$

Hybrid Direct/Indirect Approach

In general, an optimal control problem may be solved using either a direct or indirect method. An indirect method involves applying calculus of variations principles and solving the corresponding two-point boundary value problem (2PBVP). This is usually an extremely difficult problem except in the case of a simple dynamic system. A direct method utilizes a parameterization of the control and attempts to directly reduce the performance index value at each iteration. Since our three-dimensional minimum-fuel problem involves sensitive system dynamics and a dual coordinate frame, a direct optimization method is used here. The optimal control problem is replaced with an approximate nonlinear programming problem with the continuous control history replaced with a finite number of parameters. A typical approach to parameterizing the control is to utilize linear or cubic spline interpolation through a fixed number of control points. For the long-duration spiral trajectories, this technique would require a very large number of control points for sufficient accuracy. A more efficient and accurate technique is to utilize the necessary conditions from optimal control theory[12] to parameterize the control angle time histories.[13] As a result, the optimal thrust steering angles $u^*(t)$ and $v^*(t)$ are parameterized by the costate differential equations. This parameterization feature utilizes some important aspects of an indirect approach, and therefore this method is termed a "hybrid" direct/indirect optimization approach.

Necessary Conditions from Optimal Control Theory

The costate equations and transversality conditions are used to define the steering angle time histories. The costate differential equations are derived below for the Earth-centered, rotating, spherical frame, and hence subscripts are not employed. The moon-centered costate equations are derived in a similar fashion. The transversality conditions are derived in the moon-centered, rotating, spherical frame since the terminal state constraints are expressed in terms of moon-centered state variables.

The Hamiltonian in the Earth-centered, rotating, spherical coordinate frame is

$$H = \lambda^T f \tag{33}$$

where $\lambda = [\lambda_r\ \lambda_{v_r}\ \lambda_{v_\theta}\ \lambda_{v_\phi}\ \lambda_\theta\ \lambda_\phi]^T$ is the costate vector and f is the state differential equation vector consisting of the right-hand sides of Eqs. (1–6). The costate differential equations are

$$\dot{\lambda}_r = -\frac{\partial H}{\partial r} = \lambda_{v_r}\left(\frac{v_\theta^2}{r^2} + \frac{v_\phi^2}{r^2} + \frac{\mu_m}{r_{\text{moon-S/C}}^3} - \frac{3\mu_m(r + D\cos\phi\cos\theta)^2}{r_{\text{moon-S/C}}^5} - \frac{2\mu}{r^3} - \omega^2\cos^2\phi\right) + \lambda_{v_\theta}\left(\frac{-v_r v_\theta}{r^2} + \frac{v_\theta v_\phi\sin\phi}{r^2\cos\phi} + \frac{3\mu_m Dr\sin\theta(r + D\cos\phi\cos\theta)}{r_{\text{moon-S/C}}^5}\right) + \lambda_{v_\phi}\left(\frac{-v_r v_\phi}{r^2} - \frac{v_\theta^2\sin\phi}{r^2\cos\phi} + \frac{3\mu_m D\sin\phi\cos\theta(r + D\cos\phi\cos\theta)}{r_{\text{moon-S/C}}^5} + \omega^2\cos\phi\sin\phi\right) + \lambda_\theta\frac{v_\theta}{r^2\cos\phi} + \lambda_\phi\frac{v_\phi}{r^2} \tag{34}$$

$$\dot{\lambda}_{v_r} = -\frac{\partial H}{\partial v_r} = -\lambda_r + \lambda_{v_\theta}\left(\frac{v_\theta}{r} + 2\omega\cos\phi\right) + \lambda_\phi\frac{v_\phi}{r} \tag{35}$$

$$\dot{\lambda}_{v_\theta} = -\frac{\partial H}{\partial v_\theta} = \lambda_{v_r}\left(-2\omega\cos\phi - \frac{2v_\theta}{r}\right) + \lambda_{v_\theta}\left(\frac{v_r}{r} - \frac{v_\phi\sin\phi}{r\cos\phi}\right) + \lambda_{v_\phi}\left(2\omega\sin\phi + \frac{2v_\theta\sin\phi}{r\cos\phi}\right) - \frac{\lambda_\theta}{r\cos\phi} \tag{36}$$

$$\dot{\lambda}_{v_\phi} = -\frac{\partial H}{\partial v_\phi} = -\lambda_{v_r}\frac{2v_\phi}{r} + \lambda_{v_\theta}\left(-\frac{v_\theta\sin\phi}{r\cos\phi} - 2\omega\sin\phi\right) + \lambda_\phi\frac{v_r}{r} - \frac{\lambda_\phi}{r} \tag{37}$$

$$\dot{\lambda}_\theta = -\frac{\partial H}{\partial\theta} = \lambda_{v_r}\left(\frac{-\mu_m D\cos\phi\sin\theta}{r_{\text{moon-S/C}}^3} + \frac{3\mu_m(r + D\cos\phi\cos\theta)Dr\cos\phi\sin\theta}{r_{\text{moon-S/C}}^5} + \frac{\mu_m\cos\phi\sin\theta}{D^2}\right) + \lambda_{v_\theta}\left(\frac{-\mu_m D\cos\theta}{r_{\text{moon-S/C}}^3} - \frac{3\mu_m D^2 r\cos\phi\sin^2\theta}{r_{\text{moon-S/C}}^5} + \frac{\mu_m\sin\phi\cos\theta}{D^2}\right) + \lambda_{v_\phi}\left(\frac{\mu_m D\sin\phi\sin\theta}{r_{\text{moon-S/C}}^3} - \frac{3\mu_m D^2 r\cos\phi\sin\phi\cos\theta\sin\theta}{r_{\text{moon-S/C}}^5} - \frac{\mu_m\sin\phi\sin\theta}{D^2}\right) \tag{38}$$

$$\dot{\lambda}_\phi = -\frac{\partial H}{\partial \phi} = \lambda_{v_r}\left(\frac{-\mu_m D \sin\phi\cos\theta}{r^3_{\text{moon-S/C}}} + \frac{3\mu_m(r + D\cos\phi\cos\theta)Dr\sin\phi\cos\theta}{r^5_{\text{moon-S/C}}} + \frac{\mu_m \sin\phi\cos\theta}{D^2} + 2\omega^2 r\cos\phi\sin\phi + 2\omega v_\theta \sin\phi\right) + \lambda_{v_\theta}\left(-2\omega v_r \sin\phi - 2\omega v_\phi\cos\phi - \frac{v_\phi v_\theta \sin^2\phi}{r\cos^2\phi} - \frac{v_\theta v_\phi}{r} - \frac{3\mu_m D^2 r\sin\phi\cos\theta\sin\theta}{r^5_{\text{moon-S/C}}}\right) + \lambda_{v_\phi}\left(-\omega^2 r\sin^2\phi + \omega^2 r\cos^2\phi + 2\omega v_\theta\cos\phi + \frac{v_\theta^2\sin^2\phi}{r\cos^2\phi} + \frac{v_\theta^2}{r} - \frac{\mu_m D\cos\phi\cos\theta}{r^3_{\text{moon-S/C}}} + \frac{\mu_m\cos\phi\cos\theta}{D^2} - \frac{3\mu_m D^2 r\sin^2\phi\cos^2\theta}{r^5_{\text{moon-S/C}}}\right) - \lambda_\theta\frac{v_\theta\sin\phi}{r\cos^2\phi} \tag{39}$$

The transversality conditions for the moon-centered costate system define the terminal costate values in the inclined LLO:

$$\lambda_r(t_f) = \left.\frac{\partial\Phi}{\partial r}\right|_{t=t_f} + \nu^T\left.\frac{\partial\psi}{\partial r}\right|_{t=t_f} = \nu_1 \tag{40}$$

$$\lambda_{v_r}(t_f) = \left.\frac{\partial\Phi}{\partial v_r}\right|_{t=t_f} + \nu^T\left.\frac{\partial\psi}{\partial v_r}\right|_{t=t_f} = \nu_2 \tag{41}$$

$$\lambda_{v_\theta}(t_f) = \left.\frac{\partial\Phi}{\partial v_\theta}\right|_{t=t_f} + \nu^T\left.\frac{\partial\psi}{\partial v_\theta}\right|_{t=t_f} = \nu_3(2v_\theta + 2n\cos\phi) + \nu_4\cos\phi \tag{42}$$

$$\lambda_{v_\phi}(t_f) = \left.\frac{\partial\Phi}{\partial v_\phi}\right|_{t=t_f} + \nu^T\left.\frac{\partial\psi}{\partial v_\phi}\right|_{t=t_f} = 2\nu_3 v_\phi \tag{43}$$

$$\lambda_\theta(t_f) = \left.\frac{\partial\Phi}{\partial\theta}\right|_{t=t_f} + \nu^T\left.\frac{\partial\psi}{\partial\theta}\right|_{t=t_f} = 0 \tag{44}$$

$$\lambda_\phi(t_f) = \left.\frac{\partial\Phi}{\partial\phi}\right|_{t=t_f} + \nu^T\left.\frac{\partial\psi}{\partial\phi}\right|_{t=t_f} = \nu_3\left(-2n^2\cos\phi\sin\phi - 2v_\theta n\sin\phi\right) + \nu_4(-v_\theta\sin\phi - 2n\cos\phi\sin\phi) \tag{45}$$

Application of the stationarity condition yields

$$\frac{\partial H}{\partial u} = 0 = \lambda_{v_r} a_T\cos u\cos v - \lambda_{v_\theta} a_T\sin u\cos v \tag{46}$$

$$\frac{\partial H}{\partial v} = 0 = -\lambda_{v_r} a_T\sin u\sin v - \lambda_{v_\theta} a_T\cos u\sin v + \lambda_{v_\phi} a_T\cos v \tag{47}$$

The resulting direction cosines for the thrust acceleration vector components as required in the equations of motion are

$$\sin u\cos v = \frac{-\lambda_{v_r}}{\|\lambda_v\|} \tag{48}$$

$$\cos u\cos v = \frac{-\lambda_{v_\theta}}{\|\lambda_v\|} \tag{49}$$

$$\sin v = \frac{-\lambda_{v_\phi}}{\|\lambda_v\|} \tag{50}$$

where $\|\lambda_v\| = (\lambda^2_{v_r} + \lambda^2_{v_\theta} + \lambda^2_{v_\phi})^{1/2}$; the norm of the velocity costate vector $\lambda_v = [\lambda_{v_r}\ \ \lambda_{v_\theta}\ \ \lambda_{v_\phi}]^T$. The correct signs for the above direction cosines are derived by applying the strengthened Legendre–Clebsch condition, and the details are presented in Appendix B.

Solution Procedure

The requirement for the three-dimensional trajectory to terminate in a low lunar circular orbit with a prescribed inclination greatly increases the sensitivity of the problem to the initial guesses for a one-way, LEO–LLO, numerical integration. Therefore, the three-dimensional LEO–LLO trajectory is divided into two trajectory segments. The first segment starts in LEO and consists of the powered Earth-escape phase and a portion of the translunar coast phase. The second trajectory segment starts in LLO at the prescribed inclination and consists of the powered moon-capture phase and the remaining portion of the coast arc. The numerical sensitivity of the problem is further reduced by matching the two trajectory segments near the lunar sphere of influence (SOI) where the gravity fields of Earth and the moon are nearly equal. Therefore, the Earth-escape phase and initial coast arc are numerically integrated forward in time in the Earth-centered rotating frame, and the moon-capture phase and second coast arc segment are integrated backward in time from an inclined LLO in the moon-centered rotating frame. The duration of the second-coast arc segment is fixed such that the moon-based trajectory segment terminates near the SOI. The terminal position and velocity vectors from both trajectory segments must be matched in a common reference frame.

The minimum-fuel three-dimensional transfer is solved using the hybrid direct/indirect approach mentioned previously. The initial costates $\lambda_r(0)$, $\lambda_\phi(0)$, $\lambda_{v_r}(0)$, $\lambda_{v_\theta}(0)$, and $\lambda_{v_\phi}(0)$ parameterize the steering angles $u_1(t)$ and $v_1(t)$ through Eqs. (48–50) and the simultaneous forward integration of the Earth-centered state and costate equations. The unknown multipliers ν_1, ν_2, ν_3, and ν_4 parameterize the steering angles $u_3(t)$ and $v_3(t)$ through Eqs. (48–50) and the simultaneous backward integration of the moon-centered state and costate equations. The longitude angle costate λ_θ is zero at LEO since the initial longitude angle is free, and λ_θ is zero at the final inclined lunar orbit due to the fifth transversality condition [Eq. (44)].

The optimization problem is solved using sequential quadratic programming (SQP), which is a constrained parameter optimization method.[14] The SQP algorithm used is DNCONF from the International Mathematics and Statistics Library (IMSL).[15] This SQP code is based on Schittkowski's nonlinear programming code NLPQL and internally calculates gradient estimates based on first-order forward differences. SQP requires a numerical simulation with explicit computation of the performance index and constraints that result from the current design variables or optimization parameters. For the three-dimensional minimum-fuel problem, the SQP formulation has 15 design variables: the initial and final longitude angle in LEO and LLO, the final latitude of the spacecraft in inclined LLO, the five unknown initial costates in LEO, the four unknown multipliers at $t = t_f$, the durations of the powered escape and capture spirals, and the duration of the Earth-centered coast arc. The SQP problem has six equality constraints that require position and velocity matching near the lunar SOI.

The optimal three-dimensional transfer to a polar lunar orbit is obtained by starting with a planar Earth–moon trajectory and solving a sequence of minimum-fuel problems with increasing final inclination at LLO. The planar minimum-fuel solution from Ref. 10 is utilized to provide a good initial guess for the design vector for the first minimum-fuel three-dimensional problem. A good initial guess is especially required for the sensitive costate variables. The solution process could benefit from a costate control transformation.[13] This technique has been utilized by the authors in Ref. 16 for Earth–moon transfers using a more realistic electric propulsion system. The backward integration from LLO starts from a circular orbit with a desired fixed inclination. The longitude in LLO is free, and the latitude in LLO is between plus or minus the prescribed inclination. These two design variables determine the orientation of the inclined LLO and the velocity components along the longitude and latitude directions (v_θ and v_ϕ). The LLO latitude is constrained by

using upper and lower design variable box constraints in the SQP problem formulation.

Numerical Results

The desired final inclination of the lunar orbit is set at 5 deg for the first three-dimensional problem. Therefore, the planar solution initial guess results in position and velocity vector errors at the SOI match point for the first iteration. The hybrid direct/indirect method converges to the minimum-fuel solution with 5 deg final inclination in 15 iterations.

Next, a sequence of intermediate three-dimensional problems with increased lunar inclination is solved. In order to maintain desirable convergence properties, the final lunar inclination is incremented by 5 deg, and the current solution is used as the initial guess for the next three-dimensional problem. This procedure works very nicely until the final lunar inclination reaches 85 deg. The three-dimensional, three-body dynamics in the moon-centered, rotating, spherical frame become more sensitive as inclination increases, and therefore the problem is solved in 1 deg increments to a final inclination of 87 deg and in half-degree increments to the full polar lunar orbit. This numerical sensitivity is attributed to the singularity in the spherical coordinate frame at a latitude angle $\phi = 90$ deg. Consequently, during the numerical integration the dynamics become very sensitive when ϕ is near 90 deg.

The range of minimum-fuel trajectories from the planar solution to the three-dimensional polar solution is presented in Fig. 1. The optimal spacecraft mass in LLO is plotted against the final lunar inclination. The rate of performance loss steadily increases with inclination. The resulting optimal spacecraft mass in polar LLO is 93,050.4 kg. The minimum-fuel polar trajectory results in a final-to-initial mass ratio of 0.9305. The optimal three-dimensional trajectory to polar lunar orbit requires only 41.6 kg more fuel than the minimum-fuel planar trajectory. This is only 0.6% more fuel than the two-dimensional minimum-fuel solution.

The optimal three-dimensional trajectory to polar lunar orbit is shown in the Earth-centered rotating frame in Figs. 2 and 3. Figure 2 presents the projection of the three-dimensional trajectory onto the x–y Earth–moon plane, and Fig. 3 shows the projection onto the vertical x–z plane. The complete optimal three-dimensional trajectory is presented in Fig. 4 with the vertical z axis distorted in order to emphasize the vertical out-of-plane motion. The optimal trajectory completes 12 revolutions about the Earth during a 2.24-day escape spiral. At the end of the Earth-escape spiral, the orbit is inclined 2.8 deg with respect to Earth. The spacecraft is "lofted" above the Earth–moon plane during the 4.82-day coast arc, as indicated by Fig. 3. The vertical z axis is also elongated in Fig. 3 in order to emphasize out-of-plane motion. The spacecraft reaches a peak of over 2.6 Earth radii above the Earth–moon plane during the coast arc. Shortly after the vertical peak of the coast trajectory, the spacecraft coasts toward the Earth–moon plane, and the moon-capture spiral is initiated. At this point, the spacecraft is "above" the moon's orbit with an inclination of 89.2 deg. The moon-capture spiral lasts for 10.90 h and completes the slight plane change to the desired 90 deg polar lunar orbit. The final polar lunar orbit is nearly perpendicular to the Earth–moon line with a final ascending node longitude of 275.5 deg. Therefore, at the instant of injection into the circular polar lunar orbit, the angular momentum vector is pointing away from Earth and is very nearly collinear with the Earth–moon line.

The optimal thrust steering angle time histories for the Earth-escape spiral are shown in Fig. 5. The thrust steering angles u^* and v^* are resolved into in-plane and out-of-plane steering angles. The in-plane steering angle δ and out-of-plane steering angle ϵ are with respect to the instantaneous orbit plane. The longitude and in-plane steering angles u^* and δ in Fig. 5 nearly coincide for the Earth-escape spiral and resemble the profile for the planar case. The latitude and

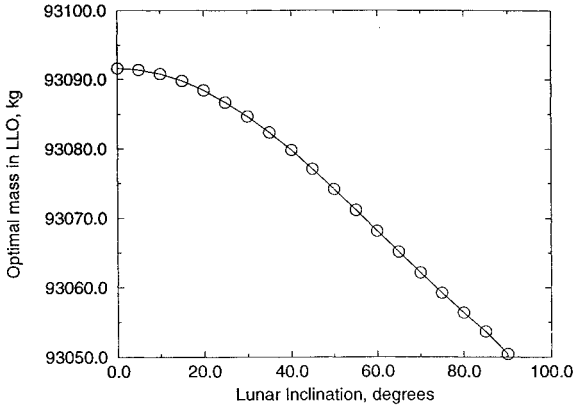

Fig. 1 Optimal mass in LLO vs lunar inclination.

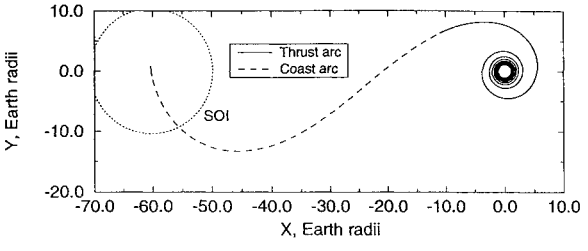

Fig. 2 Minimum-fuel three-dimensional trajectory (x–y plane), rotating frame.

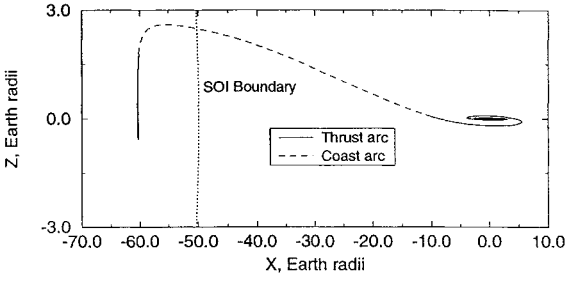

Fig. 3 Minimum-fuel three-dimensional trajectory (x–z plane) rotating frame.

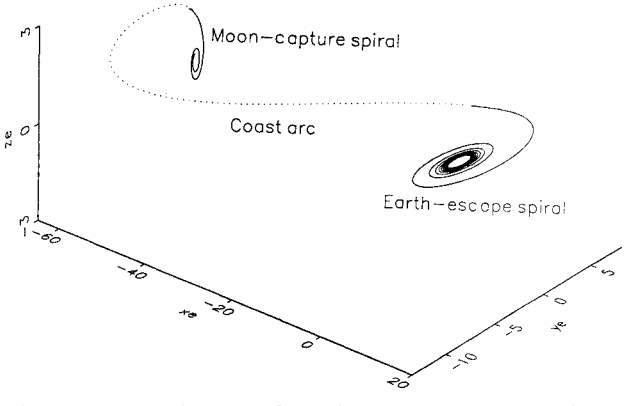

Fig. 4 Minimum-fuel three-dimensional trajectory, rotating frame.

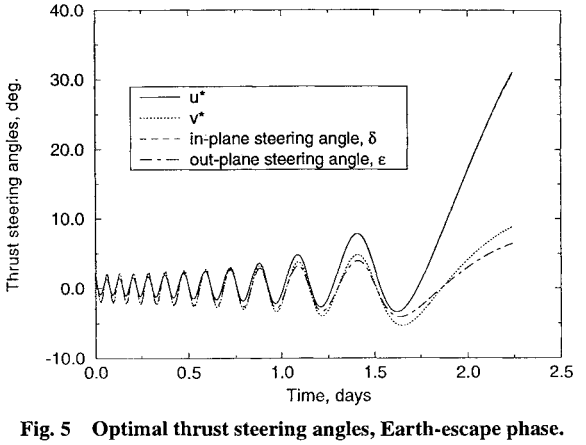

Fig. 5 Optimal thrust steering angles, Earth-escape phase.

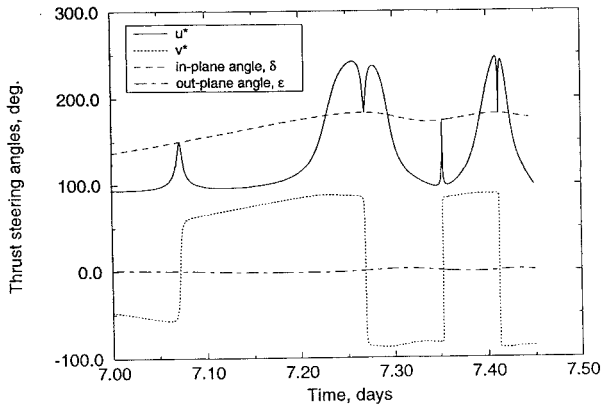

Fig. 6 Optimal thrust steering angles, moon-capture phase.

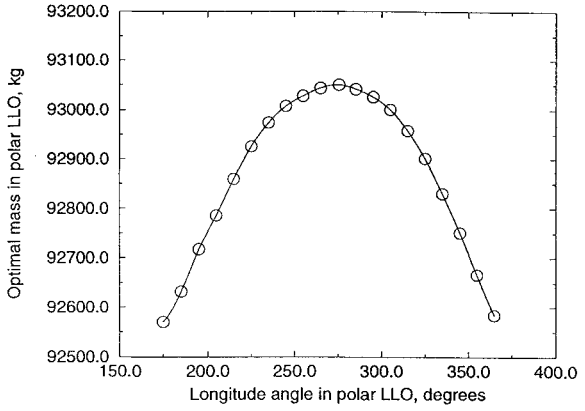

Fig. 7 Optimal mass in polar LLO, meridian constraints.

out-of-plane steering angles v^* and ϵ differ at the end of the escape spiral as the inclination increases.

The optimal steering angle time histories for the moon-capture spiral are shown in Fig. 6. The thrust steering angles u^* and v^* are again resolved into in-plane and out-of-plane steering angles. The longitude and latitude steering angles u^* and v^* display complex and discontinuous time histories. The steering angles u^* and v^* are resolved from the direction cosines, which in turn are governed by the velocity costates. When u^* and v^* are resolved into in-plane and out-of-plane steering angles δ and ϵ as shown by Fig. 6, the time histories are smooth. The discontinuities in u^* and v^* occur at the peaks and valleys of the in-plane steering angle and at the points where the out-of-plane angle is zero. The in-plane steering angle resembles the planar moon-capture profile, and the out-of-plane angle is very small. This is reasonable since the moon-capture spiral is nearly contained in a vertical plane, and the required plane change is only 0.8 deg.

Final Meridian Constraints

For a lunar cargo mission there may exist requirements that the initial polar orbit coexist with a desired vertical plane with respect to the rotating Earth–moon line for communication or rendezvous purposes. This meridian plane for a polar orbit is defined by the longitude angle θ. The effects of constraining the meridian at polar LLO insertion are investigated in this section.

The meridian constraint in LLO adds a fifth terminal state constraint to the previous minimum-fuel three-dimensional problem:

$$\psi_5 = \theta(t_f) - \theta_f = 0 \tag{51}$$

where θ_f is the desired final longitude angle or desired meridian plane. This additional terminal state constraint results in a new transversality condition for the longitude angle costate:

$$\lambda_\theta(t_f) = \left.\frac{\partial \Phi}{\partial \theta}\right|_{t=t_f} + \nu^T \left.\frac{\partial \psi}{\partial \theta}\right|_{t=t_f} = \nu_5 \tag{52}$$

Therefore, one additional design variable for ν_5 and one additional SQP equality constraint for the meridian constraint are added to the minimum-fuel hybrid direct/indirect problem formulation. Although it is possible to immediately satisfy the added meridian constraint (51) since the final longitude angle $\theta(t_f)$ is a design variable, this strategy is not employed. The final longitude angle in LLO is retained as a design variable so that the previous minimum-fuel polar orbit solution may be utilized as an accurate initial guess. The free-meridian minimum-fuel solution results in a longitude angle in LLO of 275.5 deg, and the longitude angle for the first constrained-meridian problem is fixed at 285 deg. Therefore, the initial guess for the minimum-fuel, constrained-meridian problem satisfies the six constraints for position and velocity matching on the first iteration but does not initially satisfy the meridian constraint. This problem formulation, with its 16 design variables and 7 equality constraints, provides a more robust process for obtaining the new constrained-meridian solutions.

A set of minimum-fuel, constrained-meridian problems is solved with the desired longitude angle incremented by 10 deg between problems. The complete 360 deg sweep for meridian constraints is not investigated; instead, a 190 deg range from 175 to 365 deg is investigated. The minimum-fuel meridian constraint solutions are presented in Fig. 7, which displays optimal final mass in polar LLO for the respective constrained longitude angle. The figure shows that the meridian constraint solutions are nearly symmetric about the free-meridian solution and that a substantial performance loss exists when the meridian at LLO insertion is aligned with the Earth–moon line. The constrained-meridian solution with a final longitude angle of 180 or 360 deg requires over 450 kg or 6.5% more fuel than the free-meridian solution.

Conclusions

Minimum-fuel, three-dimensional Earth–moon trajectories between inclined, circular, terminal orbits have been computed for a low-thrust spacecraft with an initial thrust-to-weight ratio of 3×10^{-3} and a fixed thrust–coast–thrust sequence. Restricted three-body problem dynamics are used for the equations of motion. The minimum-fuel Earth–moon transfer to a polar lunar orbit has been obtained by utilizing the planar minimum-fuel solution and solving a sequence of problems with increasing inclination. Minimum-fuel three-dimensional transfers to a polar lunar orbit with meridian plane constraints have also been obtained. The minimum-fuel three-dimensional problems are solved using a hybrid direct/indirect method that utilizes the benefits of a direct method and an indirect method. The costate equations are used to parameterize the thrust steering angles very accurately according to optimal control theory. The convergence sensitivity associated with satisfying the circular LLO terminal state constraints is avoided by matching a powered Earth-escape trajectory segment and a powered moon-capture trajectory segment near the lunar sphere of influence.

Surprisingly, the minimum-fuel three-dimensional transfer to a polar lunar orbit requires only 0.6% more fuel than the planar solution. A slight plane change during the powered Earth-escape phase of only 2.8 deg sufficiently "lofts" the coasting translunar trajectory above the Earth–moon orbit plane and results in a nearly vertical-plane powered moon-capture spiral trajectory. Therefore, the individual powered spiral trajectory phases are very similar to the respective Earth-escape and moon-capture phases from the planar solution. The minimum-fuel trajectory results in a final polar lunar orbit that is nearly perpendicular to the Earth–moon line. When the final meridian plane is constrained to be nearly aligned with the Earth–moon line, the resulting minimum-fuel trajectory requires about 6.5% more fuel than the free-meridian solution.

The governing dynamics formulated in a spherical coordinate frame become sensitive as the inclination approaches 90 deg. To circumvent this sensitivity, the problem could be formulated in a Cartesian frame at the expense of numerical efficiency due to the multiple revolutions. Other coordinate frames, such as the nonsingular Euler parameter set, could be utilized for this problem.

Appendix A: Coordinate Transformation

The coordinate transformation between the Earth-centered and moon-centered rotating spherical frames as represented by the functional relation $g(x_2(\tau), D)$ in Eq. (26) is presented. At the initiation of the moon-capture phase ($t = \tau$), the Earth-centered states are transformed into a moon-centered, rotating, Cartesian frame:

$$x_3 = r_2 \cos\theta_2 \cos\phi_2 + D \tag{A1}$$

$$y_3 = r_2 \sin\theta_2 \cos\phi_2 \tag{A2}$$

$$z_3 = r_2 \sin\phi_2 \tag{A3}$$

$$\dot{x}_3 = v_{r_2} \cos\theta_2 \cos\phi_2 - v_{\theta_2} \sin\theta_2 - v_{\phi_2} \cos\theta_2 \sin\phi_2 \tag{A4}$$

$$\dot{y}_3 = v_{r_2} \sin\theta_2 \cos\phi_2 + v_{\theta_2} \cos\theta_2 - v_{\phi_2} \sin\theta_2 \sin\phi_2 \tag{A5}$$

$$\dot{z}_3 = v_{r_2} \sin\phi_2 + v_{\phi_2} \cos\phi_2 \tag{A6}$$

The states in the moon-centered, rotating, Cartesian frame are then transformed into the moon-centered, rotating, spherical frame:

$$r_3 = \left(x_3^2 + y_3^2 + z_3^2\right)^{\frac{1}{2}} \tag{A7}$$

$$\theta_3 = \tan^{-1}(y_3/x_3) \tag{A8}$$

$$\phi_3 = \sin^{-1}(z_3/r_3) \tag{A9}$$

$$v_{r_3} = \dot{x}_3 \cos\theta_3 \cos\phi_3 + \dot{y}_3 \sin\theta_3 \cos\phi_3 + \dot{z}_3 \sin\phi_3 \tag{A10}$$

$$v_{\theta_3} = -\dot{x}_3 \sin\theta_3 + \dot{y}_3 \cos\theta_3 \tag{A11}$$

$$v_{\phi_3} = -\dot{x}_3 \cos\theta_3 \sin\phi_3 - \dot{y}_3 \sin\theta_3 \sin\phi_3 + \dot{z}_3 \cos\phi_3 \tag{A12}$$

Appendix B: Optimal Three-Dimensional Steering Control

In this Appendix, the optimal three-dimensional thrust steering control is developed. The thrust acceleration components required for the three-body equations of motion in a spherical frame are

$$a_{T_r} = a_T \sin u \cos v \tag{B1}$$

$$a_{T_\theta} = a_T \cos u \cos v \tag{B2}$$

$$a_{T_\phi} = a_T \sin v \tag{B3}$$

The stationarity condition for the steering angle u [Eq. (46)] results in

$$\frac{\partial H}{\partial u} = 0 \Rightarrow \frac{\sin u}{\cos u} = \frac{\lambda_{v_r}}{\lambda_{v_\theta}} \tag{B4}$$

Solving for $\sin^2 u$ yields

$$\sin^2 u = \frac{\lambda_{v_r}^2}{\lambda_{v_\theta}^2} \cos^2 u = \frac{\lambda_{v_r}^2}{\lambda_{v_\theta}^2}(1 - \sin^2 u) \tag{B5}$$

or

$$\sin u = \frac{\pm\lambda_{v_r}}{\left(\lambda_{v_r}^2 + \lambda_{v_\theta}^2\right)^{\frac{1}{2}}} \tag{B6}$$

Similarly, solving Eq. (B4) for $\cos u$ results in

$$\cos u = \frac{\pm\lambda_{v_\theta}}{\left(\lambda_{v_r}^2 + \lambda_{v_\theta}^2\right)^{\frac{1}{2}}} \tag{B7}$$

To obtain the correct sign, the strengthened Legendre–Clebsch condition[12] is enforced:

$$\frac{\partial^2 H}{\partial u^2} > 0 \qquad 0 \le t \le t_f \tag{B8}$$

Therefore, using Eq. (B4) and taking the partial derivative with respect to u yields

$$\frac{\partial^2 H}{\partial u^2} = -\lambda_{v_r} a_T \sin u \cos v - \lambda_{v_\theta} a_T \cos u \cos v > 0 \tag{B9}$$

Since the steering angle v is in the first or fourth quadrant, $\cos v$ is always nonnegative and can be divided out. Dividing out a_T and substituting Eqs. (B6) and (B7) result in

$$\frac{\partial^2 H}{\partial u^2} = -\lambda_{v_r} \frac{\pm\lambda_{v_r}}{\left(\lambda_{v_r}^2 + \lambda_{v_\theta}^2\right)^{\frac{1}{2}}} - \lambda_{v_\theta} \frac{\pm\lambda_{v_\theta}}{\left(\lambda_{v_r}^2 + \lambda_{v_\theta}^2\right)^{\frac{1}{2}}} > 0 \tag{B10}$$

Choosing the negative sign in the expressions for $\sin u$ and $\cos u$ results in

$$\frac{\partial^2 H}{\partial u^2} = \frac{\lambda_{v_r}^2 + \lambda_{v_\theta}^2}{\left(\lambda_{v_r}^2 + \lambda_{v_\theta}^2\right)^{\frac{1}{2}}} = \left(\lambda_{v_r}^2 + \lambda_{v_\theta}^2\right)^{\frac{1}{2}} > 0 \tag{B11}$$

Therefore, using the negative sign in Eqs. (B6) and (B7) satisfies the strengthened Legendre–Clebsch condition.

The stationarity condition for the steering angle v is

$$\frac{\partial H}{\partial v} = 0 = -\lambda_{v_r} a_T \sin u \sin v - \lambda_{v_\theta} a_T \cos u \sin v + \lambda_{v_\phi} a_T \cos v \tag{B12}$$

Substituting Eqs. (B6) and (B7) with the proper signs yields

$$\sin v \frac{\lambda_{v_r}^2 + \lambda_{v_\theta}^2}{\left(\lambda_{v_r}^2 + \lambda_{v_\theta}^2\right)^{\frac{1}{2}}} = -\lambda_{v_\phi} \cos v \tag{B13}$$

Solving for $\sin^2 v$ results in

$$\sin^2 v = \frac{\lambda_{v_\phi}^2}{\lambda_{v_r}^2 + \lambda_{v_\theta}^2}(1 - \sin^2 v) \tag{B14}$$

or

$$\sin v = \frac{\pm\lambda_{v_\phi}^2}{\|\lambda_v\|} \tag{B15}$$

Solving for $\cos v$ using Eqs. (B13) and (B15) yield

$$\cos v = \frac{\pm\left(\lambda_{v_r}^2 + \lambda_{v_\theta}^2\right)^{\frac{1}{2}}}{\|\lambda_v\|} \tag{B16}$$

Since $\cos v$ is always nonnegative, the positive sign in Eq. (B16) is used.

The strengthened Legendre–Clebsch condition is applied to yield

$$\frac{\partial^2 H}{\partial v^2} = -\lambda_{v_r} a_T \sin u \cos v - \lambda_{v_\theta} a_T \cos u \cos v - \lambda_{v_\phi} a_T \sin v > 0 \tag{B17}$$

Substituting Eqs. (B6) and (B7) with the negative sign for $\sin u$ and $\cos u$ and Eq. (B16) with the positive sign for $\cos v$ results in

$$\frac{\partial^2 H}{\partial v^2} = \frac{\lambda_{v_r}^2 + \lambda_{v_\theta}^2}{\|\lambda_v\|} - \lambda_{v_\phi} \sin v > 0 \tag{B18}$$

To ensure that the second partial derivative of H with respect to v is always positive, the negative sign for $\sin v$ is chosen:

$$\sin v = \frac{-\lambda_{v_\phi}}{\|\lambda_v\|} \tag{B19}$$

The direction cosines for Eqs. (B1–B3) can now be developed from Eqs. (B6) and (B7) with negative signs, Eq. (B16) with a positive sign, and Eq. (B19):

$$a_{T_r} = a_T \sin u \cos v = a_T \frac{-\lambda_{v_r}}{\|\lambda_v\|} \tag{B20}$$

$$a_{T_\theta} = a_T \cos u \cos v = a_T \frac{-\lambda_{v_\theta}}{\|\lambda_v\|} \tag{B21}$$

$$a_{T_\phi} = a_T \sin v = a_T \frac{-\lambda_{v_\phi}}{\|\lambda_v\|} \tag{B22}$$

Acknowledgments

This research was performed under the NASA Graduate Student Researchers Program and Grant NGT-50637. The authors thank John Riehl at the NASA Lewis Research Center for his suggestions and contributions to this research project.

References

[1]Jones, R. M., "Comparison of Potential Electric Propulsion Systems for Orbit Transfer," *Journal of Spacecraft and Rockets*, Vol. 21, No. 1, 1984, pp. 88–95.

[2]Hermel, J., Meese, R. A., Rogers, W. P., Kushida, R. O., Beattie, J. R., and Hyman, J., "Modular, Ion-Propelled, Orbit-Transfer Vehicles," *Journal of Spacecraft and Rockets*, Vol. 25, No. 5, 1988, pp. 368–374.

[3]Hack, K. J., George, J. A., and Dudzinski, L. A., "Nuclear Electric Propulsion Mission Performance for Fast Piloted Mars Missions," AIAA Paper 91-3488, Sept. 1991.

[4]Hack, K. J., George, J. A., Riehl, J. P., and Gilland, J. H., "Evolutionary Use of Nuclear Electric Propulsion," AIAA Paper 90-3821, Sept. 1990.

[5]Aston, G., "Ferry to the Moon," *Aerospace America*, Vol. 25, No. 6, 1987, pp. 30–32.

[6]London, H. S., "A Study of Earth-Satellite to Moon-Satellite Transfers Using Nonchemical Propulsion Systems," United Aircraft Corp. Research Dept., Rept. R-1383-1, East Hartford, CT, 1959.

[7]Stuhlinger, E., *Ion Propulsion for Spaceflight*, McGraw–Hill, New York, 1964.

[8]Golan, O. M., and Breakwell, J. V., "Minimum Fuel Lunar Trajectories for Low-Thrust Power-Limited Spacecraft," AIAA Paper 90-2975, Aug. 1990.

[9]Enright, P. J., and Conway, B. A., "Discrete Approximations to Optimal Trajectories Using Direct Transcription and Nonlinear Programming," *Journal of Guidance, Control, and Dynamics*, Vol. 15, No. 4, 1992, pp. 994–1002.

[10]Pierson, B. L., and Kluever, C. A., "Three-Stage Approach to Optimal Low-Thrust Earth–Moon Trajectories," *Journal of Guidance, Control, and Dynamics*, Vol. 17, No. 6, 1994, pp. 1275–1282.

[11]Szebehely, V. G., *Theory of Orbits, the Restricted Problem of Three Bodies*, 1st ed., Academic, New York, 1967.

[12]Bryson, A. E., Jr., and Ho, Y. C., *Applied Optimal Control*, Hemisphere, New York, 1975.

[13]Dixon, L. C. W., and Bartholomew-Biggs, M. C., "Adjoint-Control Transformations for Solving Practical Optimal Control Problems," *Optimal Control Applications and Methods*, Vol. 2, No. 4, 1981, pp. 365–381.

[14]Pierson, B. L., "Sequential Quadratic Programming and Its Use in Optimal Control Model Comparisons," *Optimal Control Theory and Economic Analysis*, Vol. 3, North-Holland, Amsterdam, 1988, pp. 175–193.

[15]International Mathematics and Statistics Library, *User's Manual*, Version 1.1, Jan. 1989.

[16]Kluever, C. A., and Pierson, B. L., "Vehicle-and-Trajectory Optimization of Nuclear Electric Spacecraft for Lunar Missions," *Journal of Spacecraft and Rockets*, Vol. 32, No. 1, 1995, pp. 126–132.